Snow cover and vegetation-induced decrease in global albedo from 2002 to 2016

AGU PUBLICATIONS

JGR

Journal of Geophysical Research: Atmospheres

RESEARCH ARTICLE
10.1002/2017JD027010

Key Points:
- Albedo decreased in high latitudes while increased in midlatitudes
- Snow cover decreased in both midlatitude and high latitudes in Northern Hemisphere. Greening happened around the world
- The dominant factors for the albedo change were snow and vegetation in midlatiude and high latitude, respectively

Correspondence to:
M. Ma and H. Yang,
mmg@swu.edu.cn;
hongyanghy@gmail.com

Citation:
Li, Q., Ma, M., Wu, X., & Yang, H. (2018). Snow cover and vegetation-induced decrease in global albedo from 2002 to 2016. *Journal of Geophysical Research: Atmospheres*, *123*, 124–138. https://doi.org/10.1002/2017JD027010

Received 21 APR 2017
Accepted 29 NOV 2017
Accepted article online 2 DEC 2017
Published online 9 JAN 2018

Snow Cover and Vegetation-Induced Decrease in Global Albedo From 2002 to 2016

Qiuping Li[1], Mingguo Ma[1], Xiaodan Wu[2], and Hong Yang[1,3]

[1]Chongqing Engineering Research Center for Remote Sensing Big Data Application, School of Geographical Sciences, Southwest University, Chongqing, China, [2]State Key Laboratory of Remote Sensing Science, Institute of Remote Sensing and Digital Earth, Chinese Academy of Sciences, Beijing, China, [3]Department of Geography and Environmental Science, University of Reading, Reading, UK

Abstract Land surface albedo is an essential parameter in regional and global climate models, and it is markedly influenced by land cover change. Variations in the albedo can affect the surface radiation budget and further impact the global climate. In this study, the interannual variation of albedo from 2002 to 2016 was estimated on the global scale using Moderate Resolution Imaging Spectroradiometer (MODIS) datasets. The presence and causes of the albedo changes for each specific region were also explored. From 2002 to 2016, the MODIS-based albedo decreased globally, snow cover declined by 0.970 (percent per pixel), while the seasonally integrated normalized difference vegetation index increased by 0.175. Some obvious increases in the albedo were detected in Central Asia, northeastern China, parts of the boreal forest in Canada, and the temperate steppe in North America. In contrast, noticeable decreases in the albedo were found in the Siberian tundra, Europe, southeastern Australia, and northeastern regions of North America. In the Northern Hemisphere, the greening trend at high latitudes made more contribution to the decline in the albedo. However, the dramatic fluctuation of snow-cover at midlatitudes predominated in the change of albedo. Our analysis can help to understand the roles that vegetation and snow cover play in the variation of albedo on global and regional scales.

1. Introduction

Land surface albedo is defined as the ratio of the reflected to the incident solar radiation upon the Earth's surface and is one of the most significant climate variables (Schaaf et al., 2008), due to its role of regulating Earth's energy budget (Liang et al., 2010; Liang et al., 2013). Albedo is highly variable both spatially and temporally. Changes in the albedo can be attributed to variations in surface structures as well as the solar radiation that the land surface receives. However, albedo depends on numerous interrelated factors, such as snow cover, vegetation, soil moisture, and solar zenith angle (SZA) (Govaerts & Lattanzio, 2008; He, Liang, & Song, 2015; Loarie et al., 2011; Wielicki et al., 2005). For example, forests have a low albedo compared to other vegetation types due to their high canopy thickness and the shading effect (Jin et al., 2002). Under snow cover conditions, however, conifers often have higher albedo than broadleaf forests because intercepted snow covers the foliage (Zhang et al., 2010). Albedo also depends on the spectral and angular distributions of the incident light. However, rougher surfaces are less sensitive to SZA because their shadows will increase with the increasing SZA, which results in less diurnal variations (Dickinson, 1983). Ghimire et al. (2014) found an increase of around 0.001 in global albedo associated with land cover change from 1700 to 2005. And that caused top-of-atmosphere radiative cooling of around -0.15 W m^{-2}. Zhang et al. (2010) estimated global albedo from multiple datasets for the period of 2000–2008. Their results showed that albedo decreased by 0.01 in the Northern Hemisphere, while it increased by 0.01 in Southern Hemisphere. Davin and de Noblet-Ducoudré (2010) simulated global surface albedo since the preindustrial era using a coupled GCM. They found an increasing albedo owing to the deforestation that lowered the global temperature by -1.36 K.

Snow cover has a substantial influence on the land surface albedo, since it is highly reflective. Both the location (i.e., on or below winter canopies) and the condition (i.e., snow age, type, state, and contamination, among others) of snow can considerably alter the land surface albedo (Moody et al., 2007). Changing snow cover extent can largely vary the surface albedo since albedo of snow is much higher than that of other land cover types. The Fourth Assessment of the Intergovernmental Panel on Climate Change attributed the strength of snow-albedo feedback to the decreasing albedo due to the loss of snow cover rather than snow metamorphism (Qu & Hall, 2007). In addition, the strong positive feedback of snow (Betts & Ball, 1997; Bonan,

lii, & Thompson, 1995; Viterbo & Betts, 1999) makes it more necessary to study the correlation between the variation of albedo and snow cover. The fluctuation in snow cover extent resulted from anthropogenic warming has been studied from both observation (Kintisch, 2017) and simulation (Bintanja & Krikken, 2016) recently; warming in the Arctic (Bintanja & Krikken, 2016) is expected to bring about substantial melting of snow and ice. Yang et al. (2001) demonstrated that the snow-albedo feedback can increase surface climate anomalies related to the El Niño–Southern Oscillation in North America.

The change in vegetation associated with land cover change is another important factor that impacts albedo values (Zhang et al., 2015). Sturm (2005) were probably the first researchers to document a tremendous energy balance alteration within the tundra as a consequence of vegetation change. Many studies (Bonan, 1997; Brovkin et al., 2006; Govindasamy, Duffy, & Caldeira, 2001) revealed that historical midlatitude deforestation may have cooled down the Northern Hemisphere because of the associated enhancing albedo. Due to the notable absorptance in the photosynthetically active radiation zone of the solar spectrum, an enhancement in the normalized difference vegetation index (NDVI) is generally expected a decline in the albedo (Bounoua et al., 2000). Moreover, decreasing albedo triggers a positive radiative forcing on the climate, which can offset the negative forcing caused by carbon sequestration (Betts, 2000). When albedo decreases because of the increase of vegetation, the augmenting surface net radiation can later heat in the atmosphere, finally lead to a more warming climate and boost the growth of vegetation (Chapin 3rd et al., 2005). Hence, deforestation/afforestation is expected to be followed by an increase/decrease albedo, respectively, ultimately leading to a more intense browning/greening trend of forest (Betts, 2000).

Compared to modeled albedo, satellite remote sensing is a more effective way to obtain global albedo values in a continuous spatial and temporal way because of less limitations and uncertainties (Liang, 2007). At present, the Moderate Resolution Imaging Spectroradiometer (MODIS) satellite albedos have a lengthy time span, and this continuity can facilitate the reconstruction of a historical background of global albedo trends (Planque, Carrer, & Roujean, 2017). Also, massive validations have been performed in MODIS albedo products and MODIS albedo has been widely used as a benchmark for assessing other satellite albedo products (He et al., 2015). Therefore, in this study, MODIS datasets were used to conduct a time series analysis to estimate the variation trend of global albedo during the period of 2002–2016. We aimed to investigate the occurrence and associated reasons for variations in the surface albedo. To achieve this goal, trends and correlations of MODIS albedo, snow cover, and vegetation over the past 15 years were evaluated. Furthermore, differences in regional-scale albedo were examined.

2. Materials and Methods

2.1. Satellite Data

The MODIS datasets employed in this study provide multiresolution spatial and temporal continuous data on the global scale. The data have been evaluated globally to ensure that its accuracy can meet the needs of an analysis of spatiotemporal climate change (Zhai et al., 2014). MODIS albedo and NDVI data were obtained from the Land Processes Distributed Active Archive Center (LP DAAC) managed by the NASA Earth Science Data and Information System project. In addition, the snow cover product was obtained from the NASA National Snow and Ice Data Center. All the data are in a geographic latitude/longitude projection at 0.05° spatial resolution.

2.1.1. Albedo

The MODIS shortwave black-sky albedo (α_{bs}) and white-sky albedo (α_{ws}) products were extracted from MCD43C3 Collection 6 datasets, which were produced daily with a 16 day accumulation window at a 0.05° spatial resolution combinations. The data range from January 2002 to December 2016. Albedo was calculated as follows:

$$\text{Albedo} = (1 - s) \times \alpha_{bs} + s \times \alpha_{ws} \quad (1)$$

where s is the fraction of solar radiation that is diffuse. Several factors, including aerosol distribution and cloud cover, can influence the fraction of diffuse skylight (Zhang et al., 2010). In this study, the diffuse skylight ratio was derived using the monthly diffuse and direct downward radiation data from National Centers for Environmental Prediction (NCEP) reanalysis (Kalnay et al., 1996; He et al., 2015). The monthly diffuse skylight ratio was downscaled to 1° latitude × 1° longitude to fit the resolution of MODIS datasets. Figure 1 displays the NCEP reanalysis monthly diffuse skylight ratio of January 2005 and June 2010.

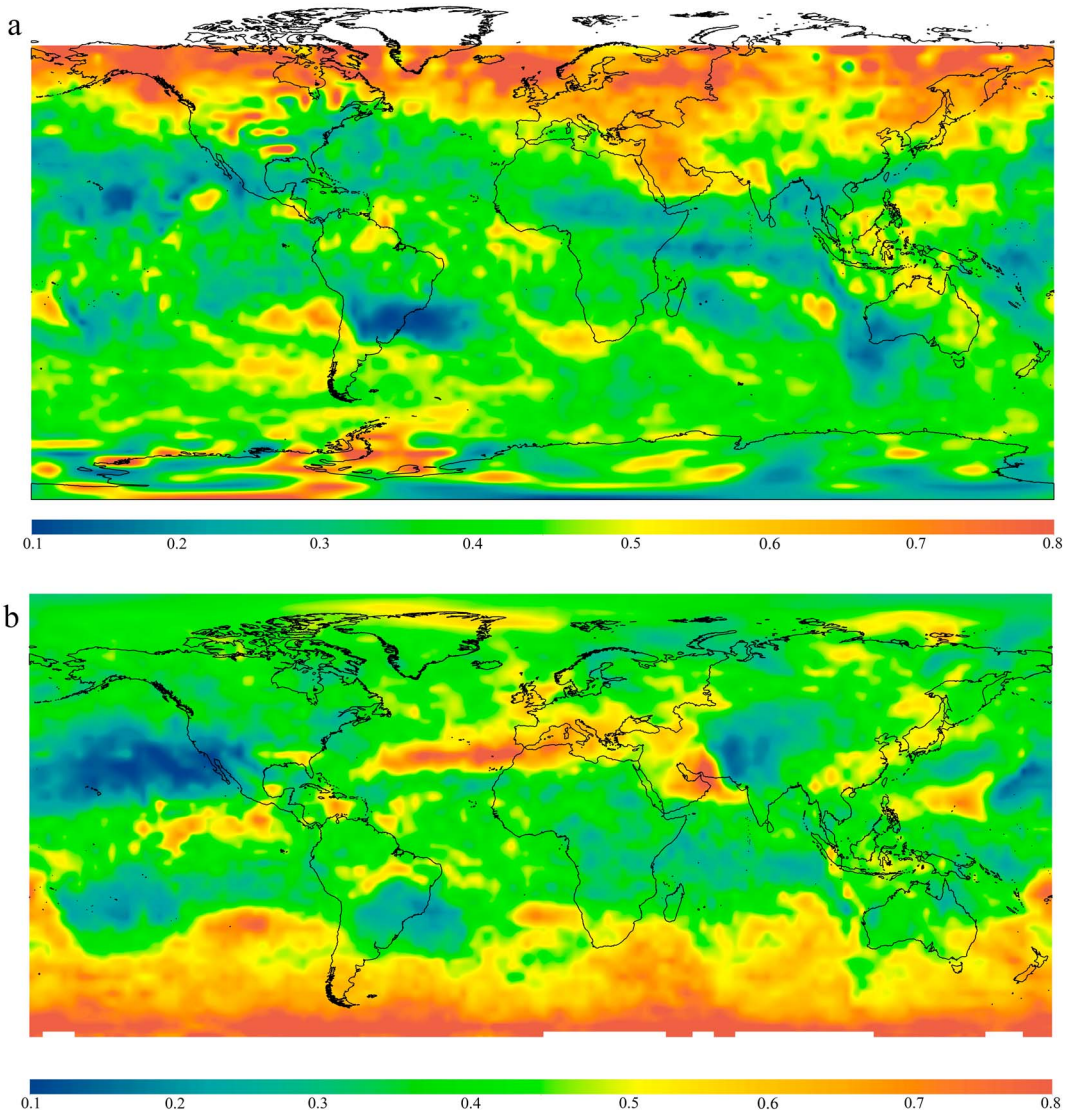

Figure 1. Global diffuse skylight ratio derived from NCEP reanalysis data in (a) January 2005 and (b) June 2010.

A quality assurance standard (NASA Land Processes Distributed Active Archive Center, 2016) was used to identify whether the albedo is characteristic of snow cover or is snow-free.

2.1.2. NDVI

The MODIS/Terra monthly NDVI product (MOD13C2, Collection 6) is based on cloud-free spatial composites of 16 day, 1 kilometer NDVI data. Data between January 2002 and December 2016 were used. Pixel reliability data were applied to determine the snow cover percentages.

Seasonally integrated normalized difference vegetation index (SINDVI) was used to characterize the global range of vegetation states and processes. The SINDVI is described by each pixel's sum of NDVI values when the NDVI exceeds a threshold value (commonly defined as NDVI $>$ 0.1) (Stow et al., 2003). In this study, only the grid cells with greater than 0.1 were used in order to eliminate the influence of bare and sparsely vegetated regions (Piao et al., 2006; Zhou et al., 2001) as well as to determine the growing season (Hope et al., 2003).

2.1.3. Snow Cover

The snow cover dataset (MOD10CM, Collection 6) was extracted from January 2002 to December 2016 to retrieve the variation trend in the snow cover. The unit of the data is percent per pixel. The product lacks data for the Antarctic. Therefore, an analysis of the Antarctic is absent in this research.

2.2. Statistical Analysis

For time series and correlation analysis, the annual values of albedo and snow cover were estimated by averaging the intra-annual data. For determining annual vegetation, the sum of NDVI (SINDVI) was used when there exists a growing season (NDVI $>$ 0.1).

2.2.1. Time Series Analysis

The slopes and ranges of the MODIS albedo, SINDVI, and snow cover were calculated respectively to estimate their variation trends during the period of 2002–2016. The changing rates were derived from the interannual variability of albedo, SINDVI, and snow cover, respectively (Stow et al., 2003). Ordinary least squares methods in the linear regression were used:

$$\text{Slope} = \frac{n \times \sum_{i=1}^{n} (i \times A_i) - \sum_{i=1}^{n} i \times \sum_{i=1}^{n} A_i}{n \times \sum_{i=1}^{n} i^2 - \left(\sum_{i=1}^{n} i\right)^2} \tag{2}$$

where n is the length of the time series that was studied; i is the number of year, $i = 1,2, \ldots, n$, in this paper, $n = 15$; and A_i means albedo, SINDVI, or snow cover in the ith year. When the slope values near 0, it means no significant changes in the trend. Slope $>$ 0 indicates an increasing trend, while slope $<$ 0 means a decreasing trend (Chen et al., 2010).

Subsequently, the ranges of variation (the total change between 2002 and 2016) in albedo, SINDVI, or snow cover were calculated:

$$\text{Range} = \text{Slope} \times (n - 1) \tag{3}$$

where n is the length of the time series.

2.2.2. Correlation and Partial Correlation

Pearson's correlation coefficients (r) were calculated between the SINDVI, snow cover, and albedo to determine their correlations on each pixel.

$$r_{XY} = \frac{\sum_{i=1}^{n} (X_i - \overline{X})(Y_i - \overline{Y})}{\sqrt{\sum_{i=1}^{n} (X_i - \overline{X})^2} \sqrt{\sum_{i=1}^{n} (Y_i - \overline{Y})^2}} \tag{4}$$

The correlation coefficient between X and Y is explained in equation (4), where X_i and Y_i are the values of the ith year and $\overline{X}$ and $\overline{Y}$ are the average values of all years.

In addition, the partial correlation was estimated in this study. Here the partial correlation coefficient ($r_{YZ \cdot X}$) was used to draw a closer link between albedo and the other two factors (SINDVI and snow cover). By calculating the partial correlation coefficient, the interaction between SINDVI and snow cover can, to some extent, be suppressed and eliminated. It means that when measuring the degree of correlation between albedo and SINDVI, the effect of snow cover can be removed:

$$r_{YZ \cdot X} = \frac{r_{YZ} - r_{YX} r_{ZX}}{\sqrt{(1 - r_{YX}^2)(1 - r_{ZX}^2)}} \tag{5}$$

where $r_{YZ \cdot X}$ represents the partial correlation coefficient between Y and Z without consideration of the impact of X and r_{ij} is the simple correlation coefficient between variables i and j. Through a comparison between the partial coefficients, we prioritized the dominant factor of each pixel.

For all correlation calculations, Student's t test was applied to assess statistical significance.

2.3. Reconstruct NDVI Data

A simple but efficient method based on a mean-value iteration filter is applied to reduce the noise and fill the gap of the monthly NDVI time series data (Ma & Veroustraete, 2006). This method has been proven to be more effective with comparison to other methods, commonly used as a reconstruction approach (Lovell & Graetz, 2001; Verhoef, Menenti, & Azzali, 1996). For each pixel, the multiyear average NDVI (ANDVI) was calculated to replace the no-data pixels for the same month. Then Δ_i was estimated as follows:

$$\Delta_i = |\text{NDVI}_i - (\text{NDVI}_{i-1} + \text{NDVI}_{i+1})/2| \tag{6}$$

where i indicates ith observation of the monthly NDVI (i varies from 1 to 180 for the 15 years). When Δ_i is greater than a threshold value, NDVI_i is replaced by $(\text{NDVI}_{i-1} + \text{NDVI}_{i+1})/2$. The threshold value ($\Delta_T$) can

be set as a small percentage of the multiyear ANDVI for each pixel. Finally, the iteration ends when all the Δ_i are less than Δ_T.

2.4. Deseasoned Anomalies

The seasonal cycle was removed by subtracting the average value for the same month over years as follows (Irwin & Oliver, 2009; Zhang et al., 2010):

$$\Delta\alpha(\mathrm{yy},\mathrm{mm}) = \alpha(\mathrm{yy},\mathrm{mm}) - \overline{\alpha}(\mathrm{mm}) \tag{7}$$

where $\Delta\alpha$(yy, mm) is the deseasoned albedo for year yy and month mm, α(yy, mm) is the monthly albedo in year "yy" and month "mm," and $\overline{\alpha}(\mathrm{mm})$ is the average albedo over 15 years for month "mm."

2.5. Experimental Design

The objectives of this research were to study the existences and causes of annual surface albedo, snow cover, and SINDVI's global trends from 2002 to 2016; to evaluate their correlations; and to explore the reasons for the variation of albedo in several significant regions.

For each pixel, the slope over the past 15 years was calculated using equation (2). Once the slopes were identified, the range of their changes was estimated following equation (3). A greater range indicates a more dramatic variation.

The zonal albedo can demonstrate a latitudinal distribution and represent the differences among different latitudinal bands. However, it is important to take the area weights into consideration when estimating the zonal value, since the outcomes derived from employing or excluding area weights are substantially different (Zhang et al., 2010). An overestimation of approximately 0.05 can arise for the global land shortwave albedo if area weights are not considered (Zhang et al., 2010). The area weights were defined as the cosine of the medial latitude of each grid to extract the approximate area-weighted albedo, SINDVI, and snow cover. This method was conducted rather than transforming all the data into a sinusoidal projection, which is a pseudo-cylindrical equal-area map projection (Zhang et al., 2010).

The MODIS albedo values, which were projected onto the nonequal-area map, were multiplied by the area weights to estimate the actual albedo values. Then, the zonal albedo of a specific area can be calculated from dividing the sum of the albedo by the sum of the area.

In addition, the correlation coefficients and partial correlation coefficients were analyzed using software SPSS 11.0 (SPSS Inc, Chicago, IL, USA) as described in equations (4) and (5) to explore how the variation of snow cover and vegetation can explain the changing albedo. The absolute values of two partial correlations, namely, the partial correlations between albedo and snow cover and between albedo and SINDVI, were compared for each pixel. The maximum coefficient was set as the primary factor that made the largest contribution to the variation of albedo (Figure 4).

3. Results

3.1. Variation Trends

The interannual variations of the albedo, SINDVI, and snow cover are shown in Figures 2a–2c. The proportion of the total increased (gray) and decreased (black) areas is shown in the underpinned inset pie chart, which can assist in comparing the percentages of increase and decrease.

Obvious increases of albedo occurred widely throughout the midlatitude and northeastern Canada. In general, 51.7% of global area experienced an upward trend of the albedo, as implied in the pie chart (Figure 2a). In Central Asia, a noticeable increment of 0.040 in the albedo was found. However, decreasing albedo was detected within most of the latitude bands. For example, albedo decreased by 0.013 in the higher latitudes of the Northern Hemisphere. However, there is no significant fluctuation of the albedo within the lower latitudes and in the southern hemisphere.

The SINDVI demonstrated a greening trend worldwide (Figure 2b), with 69.3% of the area showing an upward trend, as presented in the pie chart. Nevertheless, dramatic browning trends appeared in eastern Brazil, Argentina, northwest Canada, east coast of Africa, western Australia, and central Asia. As for the variation of snow cover extent, differences were observed among different latitudinal bands. In the Northern Hemisphere, the midlatitudes changed intensely with an average decline of 1.064. However, the higher

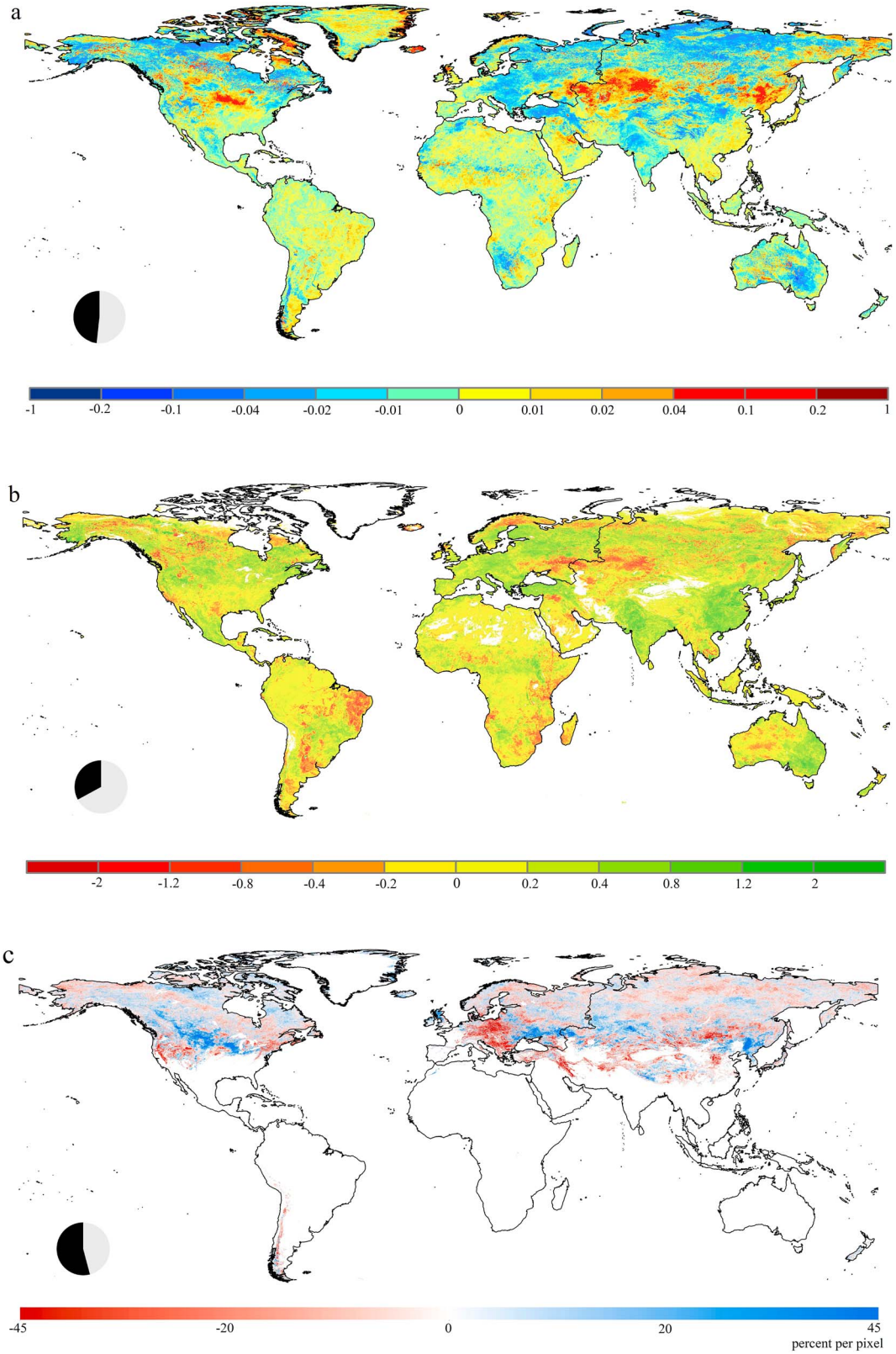

Figure 2. Ranges of (a) albedo, (b) SINDVI, and (c) snow cover during the period of 2002–2016. Continental outlines were modified from a shapefile using ArcGIS 10.3 (Environmental Systems Research Institute, Redlands, CA).

Table 1
Data for 15 Complete Years of Global and Latitudinal Ranges of the Shortwave Albedo, SINDVI and Snow Cover

	Global	60–80°N	30–60°N	10–30°N	10°N -10°S	10–30°S	30–60°S
Albedo							
Annual average	−0.0004	−0.013	0.0009[a]	0.0008[a]	0.001	−0.0004[a]	−0.001
SINDVI							
Annual average	0.175	0.156	0.256	0.227	0.061	0.057	0.176
Snow cover							
Annual average	−0.970	−0.792	−1.064	−0.964	-	-	−0.928

[a]Low confidence level.

latitudes exhibited less of the critical change, declined by 0.792 (Table 1). Slightly more than half of the global area (54.1%) displayed a declining tendency in the snow cover, which could result from global climate warming.

3.2. Correlations With SINDVI and Snow Cover

To quantify the spatial correlation coefficients between SINDVI, snow cover, and albedo, the correlation coefficients of all grid cell were calculated (Figure 3).

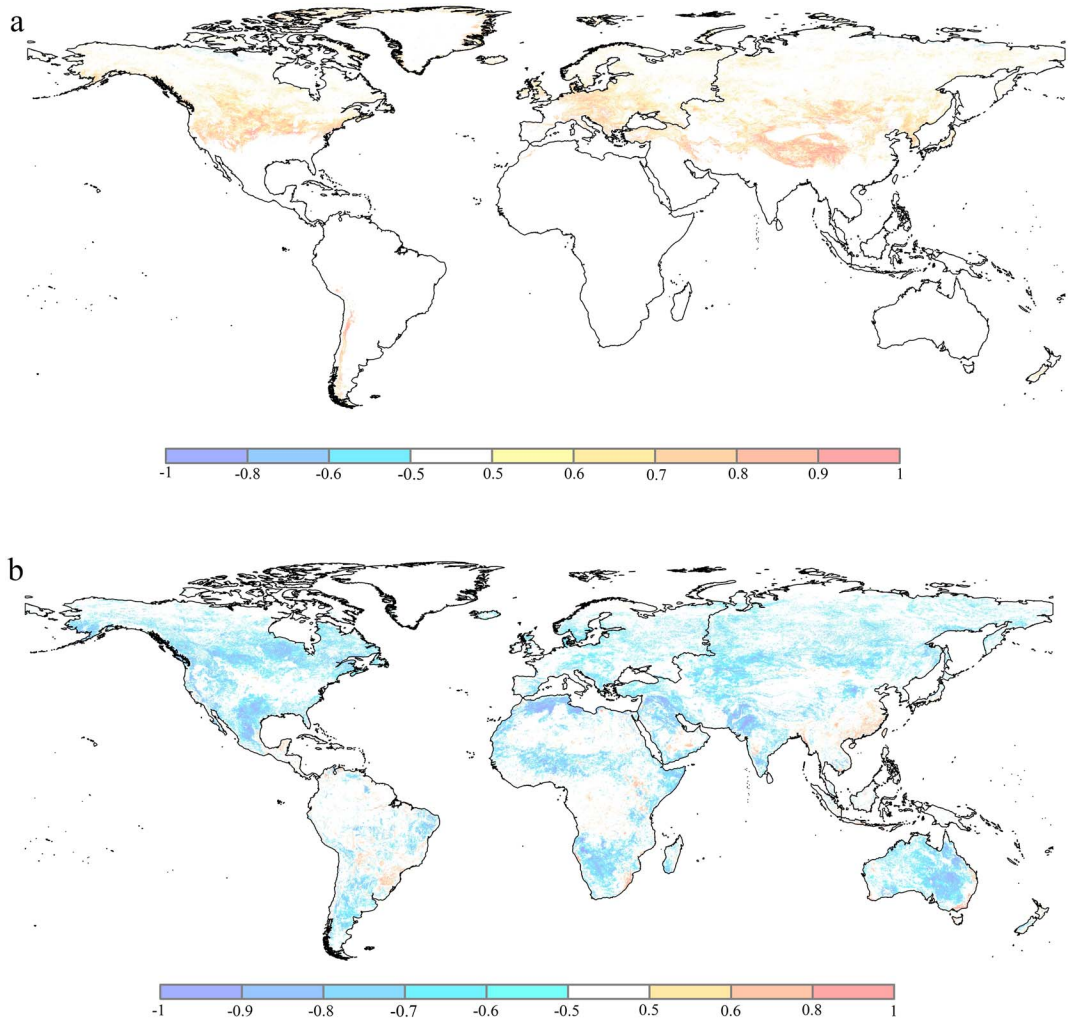

Figure 3. Spatial patterns of correlation coefficients (a) between albedo and snow cover and (b) between albedo and SINDVI. Areas with *P* values higher than 0.05 are showed in white, and the colored regions are characterized by a 95% confidence interval.

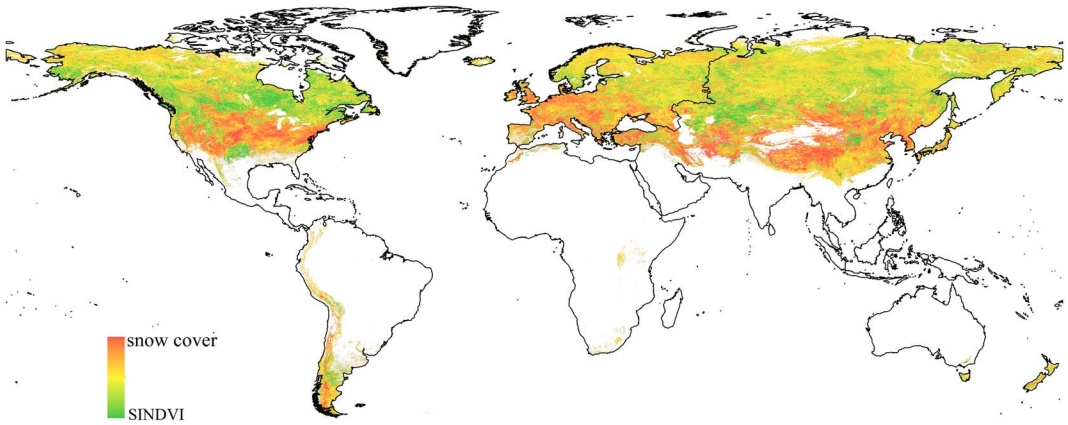

Figure 4. Spatial pattern of two variables' contributions to the change of albedo (SINDVI, green; snow cover, red). Pixel resolution: 5.6 km; period: 2002–2016. Areas with no snow cover are shown in white.

Strong positive correlations between albedo and snow cover were compromised by small area and that was found in midlatitudes in Northern Hemisphere and in the Andes in South America (Figure 3a). However, negative correlation appeared in few areas in tundra in the North Hemisphere.

There was negative correlation between albedo and SINDVI in most parts of the world except for the southeast of China, east coast of Australia, and southern Brazil where there was positive correlation. This positive correlation is different from previous knowledge. In those areas, factors other than vegetation must play a more dominant role for the change of albedo. In southeast China, the albedo product may not be perfectly convincing since a high aerosol optical depth may contaminate the observation, because insufficient clear-sky observation will result in the use of backup magnitude inversion instead of full inversion in MODIS albedo product. Magnitude inversion has lower quality that will reduce the accuracy of retrieved albedo (Jin, 2003). For MODIS NDVI, the backup approach maximum value composite (MVC) will be used when lacking of good quality observation. MVC tends to overestimate the NDVI value because the chosen maximum NDVI is not always the nadir-value (Huete et al., 2002). Thus, the less accuracy albedo and NDVI will together affect their correlation.

The partial correlation coefficients were calculated to estimate the dominant factor for each pixel using the method presented in section 2.4. A clear distribution of the dominant factor displays in Figure 4, wherein 36% of the area is significant ($p < 0.05$).

The locations where snow cover contributed more to the variation of albedo were situated in areas where snow cover changed markedly (Figures 2c and 4). In the midlatitudes, snow cover extent diminished greatly in Europe, Asia, and the coast of North America, while it increased markedly in central North America, northeastern China, and southern East European Plain. In those regions, snow cover is the primary factor influencing the variation of albedo over the period of 2002–2016. Because of the ongoing climate warming, the midlatitudes, unlike the higher latitudes where snow cover is persistent for the majority of the year, were experiencing a fluctuation in snow cover, which can dramatically change the land surface along with albedo.

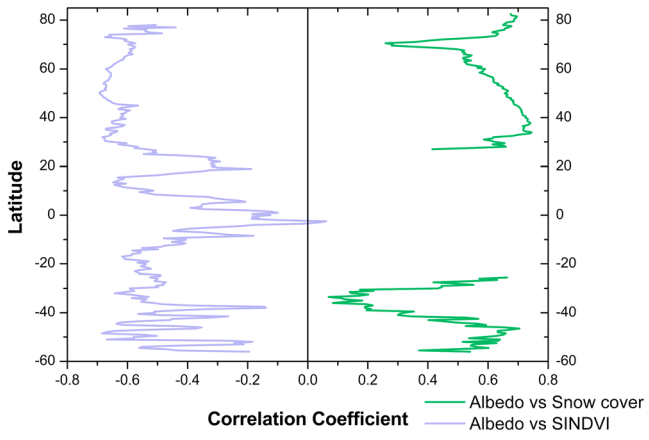

Figure 5. Correlation between SINDVI, snow cover, and albedo for latitudinal bins of 5°.

At higher latitudes, the change in vegetation contributed more to the variation of albedo in the majority of the land. In these areas, the occurrence of a greening trend (Figure 2b) implied a warming climate. In addition, the increase in vegetation led to a decrease in the albedo.

The correlations between SINDVI, snow cover, and albedo were plotted onto a latitudinal pattern (Figure 5). It is evident that snow cover had a positive correlation with the albedo, while vegetation had a negative correlation with the albedo. In the midlatitudes in Northern Hemisphere, strong negative correlations occurred between SINDVI

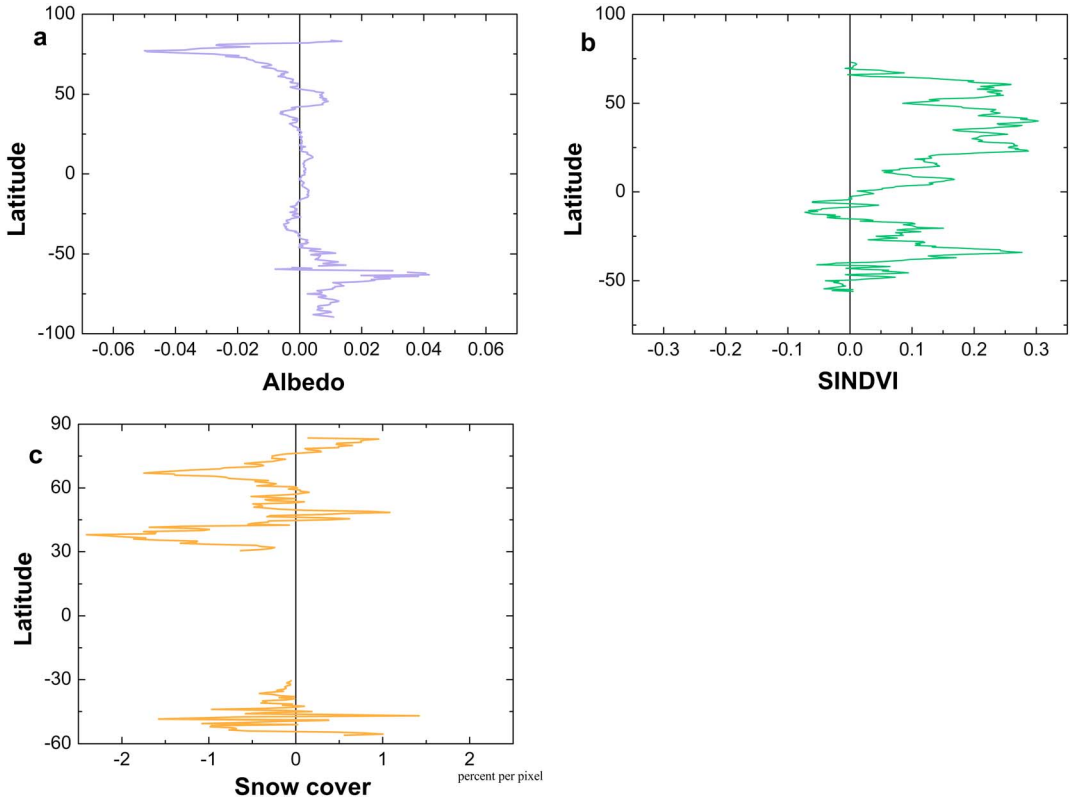

Figure 6. The latitudinal pattern of the trends for (a) albedo, (b) SINDVI, and (c) snow cover from 2002 to 2016.

and albedo. On the contrary, due to the relatively stable surface condition around the tropical regions, there is poor relation between SINDVI and albedo.

3.3. Latitudinal Variation

The plots in Figure 6 demonstrate the range of the albedo (Figure 6a), SINDVI (Figure 6b), and snow cover (Figure 6c) for latitudinal bins of 5°. The average latitudinal values featuring the area-weight were calculated. The albedo from 2002 to 2016 varied little in latitudinal pattern since the most significant change in albedo is within ±0.05. In tropics, the albedo varied slightly. As for the albedo in the high latitudes, there is an obvious decreasing trend in the Northern Hemisphere while an increasing trend in the Southern Hemisphere (Figure 6a).

The trend in the SINDVI is demonstrated in Figure 6b. The vegetation in the low latitudes diminished during the period of 2002–2016, due to rainforest deforestation (Khanna et al., 2017). In contrast, vegetation in the Northern Hemisphere expanded greatly, and a similar expansion appeared at latitudes 15°S–30°S. Meanwhile, at higher latitudes in the Southern Hemisphere, vegetation seemed to vary dynamically.

Figure 6c illustrates a noticeable decline in snow cover globally. Around 50°N, the extent of snow cover expanded slightly. However, in the midlatitudes of the Northern Hemisphere, snow cover decreased dramatically and reached its peak at 38°N with a rate of 2.4% per pixel.

3.4. Deseasoned Anomalies

In the high latitudes in Northern Hemisphere, the deseasoned albedo showed slight decrease of 0.004 from 2002 to 2016 (Figure 7a). However, opposite trend appeared in midlatitudes (Figure 7b) with an increase of 0.0009. The same pattern of SINDVI appeared in midlatitude and high latitude. But SINDVI increased more obviously in midlatitude (0.018) than in high latitude (0.007). Besides, snow cover retreated in both midlatitude and high latitude. Since a greater extent of warming appeared in high latitudes, snow cover anomalies

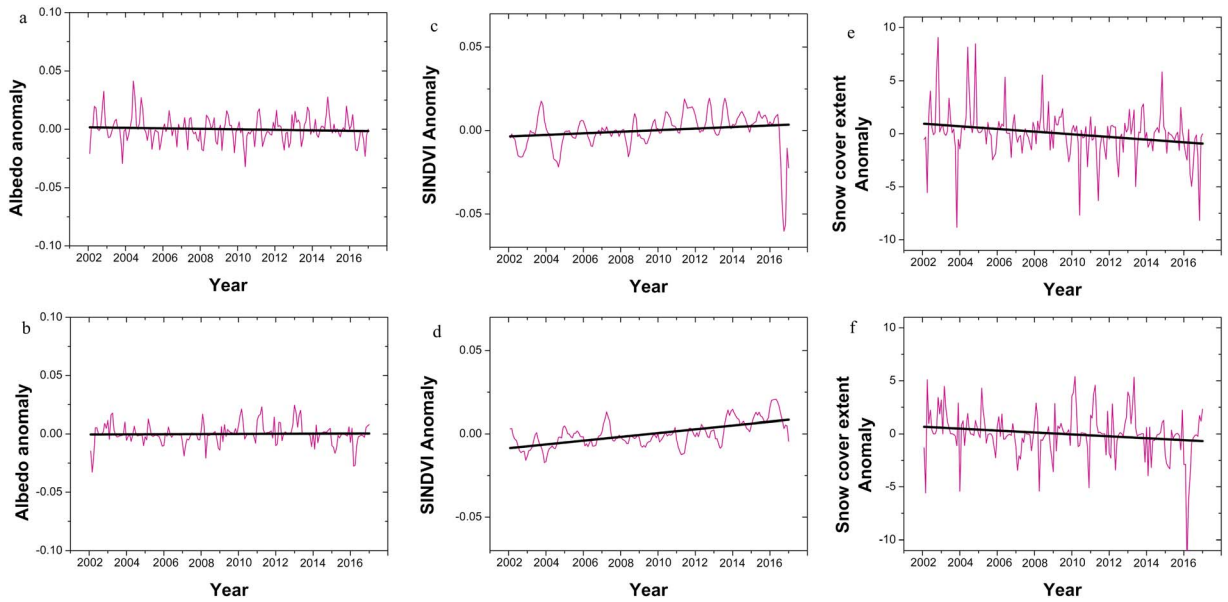

Figure 7. Albedo, SIDNVI, and snow cover anomalies for midlatitudes and high latitudes in Northern Hemisphere from 2002 to 2016. (a) High latitudes albedo. (b) Midlatitudes albedo. (c) High-latitude SINDVI. (d) Midlatitude SINDVI. (e) High-latitude snow cover. (f) Midlatitude snow cover.

decreased more intensely in high latitude (1.933) than in midlatitude (1.414). However, different from the nondeseasoned data, snow cover declined more obviously in midaltitude (Table 1).

The declining albedo in high latitude increased the stay of more solar energy on Earth, thus enhanced the warming. In midlatitudes, the increase of albedo was mainly contributed by the pronounced increase of snow cover in Central Asia, northeastern China, and central North America. However, in general, climate warming happened in midlatitude and high latitude in the Northern Hemisphere where the snow cover decreased while SINDVI increased.

3.5. Zonal Albedo

The latitudinal albedo values were summarized by separating the zones according to latitude. The latitudinal bands were divided according to zones labeled as high latitude, midlatitude, and low latitude. The range of albedo, SINDVI, and snow cover are presented in Table 1. The global albedo declined slightly by 0.0004 over the past 15 years. The most significant decrease of surface albedo lied in the high latitudes. Meanwhile, SINDVI increased globally, indicating an expansion of vegetation all over the world. While for the latitude 10°–30° S, SINDVI increased marginally by 0.057. For snow cover, a decreasing trend appeared from 2002 to 2016, especially in the 30°–60° N latitudes where snow cover decreased by 1.1% per pixel.

4. Discussion

The time series analysis of the interannual average albedo demonstrates a decreasing trend in high latitudes while increasing trend in midlatitudes over the recent years (Table 1 and Figure 7). However, a notable difference in the spatial and temporal patterns has been found around the world (Figure 2a). The albedo increased in Central Asia, especially the steppe and prairie regions, the steppe and temperate broadleaf forests in northeastern China, parts of the boreal forest in Canada, northwest Canada, the temperate steppe in North America, and eastern Siberia. Meanwhile, a decreasing trend of albedo occurred over the Siberian tundra, Europe, southeastern Australia (where most of the regions are temperate steppes), and northern North America. With regard to Greenland, the albedo increased along the east border. Despite of some increases, the albedo declined by 0.0004 on a global scale (Table 1), which indicates more solar radiative energy remained on the ground and that may make a positive contribution to global warming. (Table 2).

Table 2
Pearson's Correlation Coefficients of the Albedo, SINDVI, and Snow Cover Using the Annual Average Data

	Correlation coefficient						
	Global	60–80°N	30–60°N	10–30°N	10°N–10°S	10–30°S	30–60°S
Annual average							
Albedo versus SINDVI	−0.5651	−0.6270	−0.5630	−0.5025	−0.3055	−0.5342	−0.5251
Albedo versus Snow cover	0.6510	0.5249	0.8970	0.4807	-	0.4585	0.3438

4.1. Significant Increases in Albedo

4.1.1. Central Asia

The albedo of Central Asia ascended dramatically by 0.025 over the past 15 years. This significant increase was observed in a wide stretch of land in Central Asia (Figure 2a). The severe deforestation (Figure 2b) in this area was the main reason for the increase in albedo, which is illustrated by the partial correlation coefficient matrix (Figure 4). A warmer climate is expected to appear in the summertime, and aridity has increased over the entire region (Lioubimtseva & Henebry, 2009), which is also retrieved from the MODIS satellite data. This extreme weather brought about the downward trend in SINDVI (Figure 8). Meanwhile, the lower temperature during the winter (Lioubimtseva & Henebry, 2009) was related to the increase in snow cover (Figure 8b). This change in climate coincided with a decline in SINDVI in the summertime and an increase in snow cover during the winter. Eventually, their effects resulted in an increase in the albedo.

To further investigate the evolution of albedo, SINDVI, and snow cover extent from 2002 to 2016, a typical grassland within Central Asia (Figure 8b) was chosen to perform the time series regression. Figure 8b shows the regression slope of albedo is +0.007 (R^2 = 0.6088). What is more, SINDVI decreased noticeably (R^2 = 0.4643) while snow cover increased markedly (R^2 = 0.429).

4.1.2. North America

Pronounced increase in albedo was detected in the central and northwestern North America. In these areas, the variation of snow cover extent acted as the dominant factor that affected the albedo (Figure 4). The cooling winter especially in 2009/2010, 2010/2011, and 2013/2014 in midwest North America drew more attention to public and studies (Palmer, 2014; Yu & Zhang, 2015) because it was contradictory to anthropogenic warming. The previous research (Sigmond & Fyfe, 2016) attributed the cooling in northwest North America to the climate fluctuations especially the strengthen trade wind associated with increasing surface air temperature in the tropical Pacific and cooling in central North America to local intensified sea level pressure. Both the remote and local fluctuations led to cold temperatures and snow storms that increased the snow cover, which was also retrieved from MODIS data.

We looked into the cropland in the central North America and found two maximum values of snow cover in 2009/2010 (84.1% per pixel) and 2013/2014 (80.2% per pixel) (Figure 8d). Figure 8d displays a positive trend of snow cover in the early 21st century. Besides, albedo increased from 0.23 to 0.27 and a similar annual fluctuations were found for albedo and snow cover.

4.1.3. China

The positive correlation between albedo and SINDVI (Figure 3b) in southeastern China and Sichuan Basin was different from the general expectation that an increase in vegetation would accompany by a decrease in albedo. The variation of SINDVI (Figure 2b) demonstrated a wide range of greening in China (Lai et al., 2016). The greening has also been recorded by Xiao, Zhou, and Zhang (2015). They found the increasing air temperature explained most of the increase trend of NDVI. In addition, human activities have accelerated the greening. A mix forest area located in Sichuan Basin showed a steady increase in SINDVI with the slope of 0.09 in the period of 2002–2016 (R^2 = 0.8858) (Figure 8e). However, albedo increased from 0.104 to 0.115 in the meantime. Furthermore, the negative correlation between albedo and snow cover was also rare.

We attributed this unusual phenomenon to MODIS albedo contamination by aerosol. The dramatic increasing particulate matter 2.5 ($PM_{2.5}$) was observed from different satellite data in China. For example, the southeast China and Sichuan Basin suffered the $PM_{2.5}$ pollution (Geng et al., 2015; Peng et al., 2016). The high aerosol optical depth in China resulted from air pollution tends to reduce the number of clear-sky observations from satellite (Zhang et al., 2010). In that case, the albedo products contain some sources

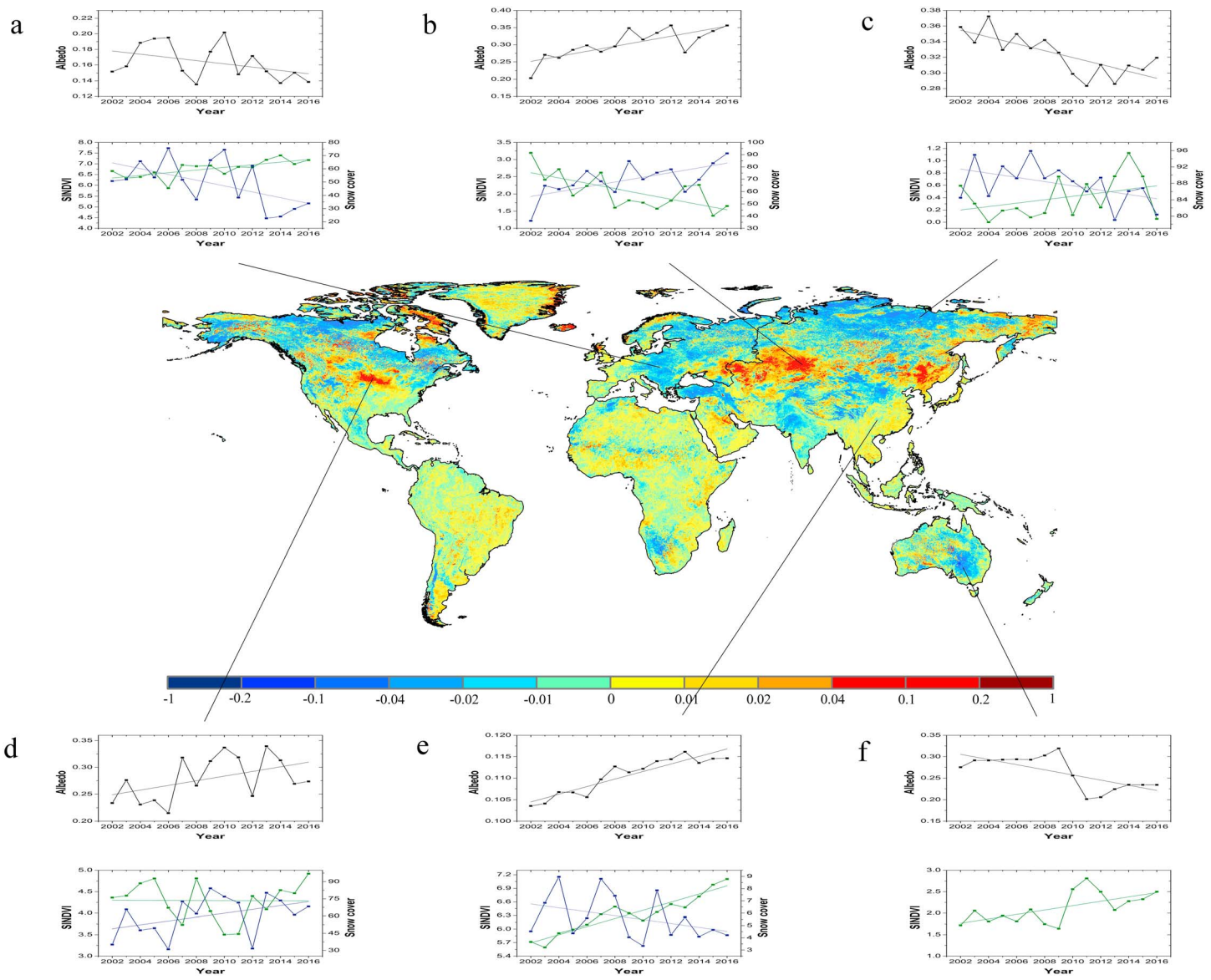

Figure 8. Time series plots of the albedo (black), SINDVI (green), and snow cover (blue) for six different regions across the world. The solid line is the linear regression of the time series. The map in the main panel insert represents the range of albedo from 2002 to 2016. Time series data are the regional average values of a 1° × 1° area (total pixels = 400). The coordinates of the lower left corner of each area are shown in parentheses. (a) Europe mixed forests (50°N, 18°E). (b) Central Asia grasslands (50°N, 77° E). (c) Arctic taiga (70°N, 115°E). (d) North America croplands (45°N, 99°W). (e) China mixed forests (26°N, 103.7°E). (f) Australia open shrub lands (31°S, 140°E).

of error and the accuracy of the result was compromised. Thus, retrieving more accurate albedo becomes a critical issue in those areas.

In southeast China, air temperature continued to increase since last century (Ji et al., 2014). Precipitation has also increased while soil moisture content decreased (Trenberth, 2011). The sufficient precipitation and high temperature contributed to the increase of SINDVI. However, the soil moisture content has decreased and this can lead to the increase of albedo in the area.

4.2. Significant Decreases in Albedo

4.2.1. Arctic

Albedo decreased widely across the northern Eurasian continent (Figure 8c). A similar dramatic decrease in the latitudinal pattern was shown in Figure 6a. Meanwhile, a greening trend was detected by regression

analysis (Figure 8c) and can been seen from the latitudinal plot (Figure 6b). The greening within the Arctic and the observed decrease in snow cover together contributed to the decreasing albedo (Figure 4). Recent studies demonstrated that the substantial melting in the Arctic happened due to the warming climate (Bintanja & Krikken, 2016; Blok et al., 2011; Kintisch, 2017; Lutz et al., 2016). Kintisch (2017) shows that not only the rising temperature but also the pigment produced by microbes and algae on the surface water boost the melting. The same decreasing snow cover was found in Arctic taiga (Figure 8c) where the regression slope of snow cover extent is −0.515 (R^2 = 0.2387). The melting snow exposed to the underneath plant, and what is more, the higher temperature in Arctic accelerated the grow rate of plant, causing the increase in SINDVI.

Furthermore, the declined in snow and ice together with the augmented vegetation reveal a less reflective surface. Thus, the land surface absorbs more solar radiation and this enhances the initial perturbation (Thackeray & Fletcher, 2016).

4.2.2. Europe

A widespread decrease in albedo values was observed from MODIS data especially in Eastern Europe (Figure 2a). In addition, greening occurred across Europe (Figure 2b). The forest in Europe served as carbon sink that mitigated some impacts of climate change (United Nations Economic Committee for Europe, 2011). A pronounced decrease in snow cover was observed in Central Europe (Figure 2c). The correlations illustrate that the variation of albedo was shaped by decreasing snow cover and increasing vegetation. However, the dramatic decrease of snow cover by 1.659 made more contribution to the decline in albedo (Figure 4).

The upward trend of downward surface solar radiation in Europe (Sanchez-Lorenzo et al., 2017) leaded to climate warming and the shrinking of snow cover. The increasing warming has been detected since last century (Ji et al., 2014). Besides, recent controversial studies (Naudts et al., 2016) concluded that additional trees in Europe have been contributing to a warming planet because of the wood extraction and tree species change (choosing conifers over broadleaved varieties). That point of view may somewhat explain the decrease in snow cover over Europe where greening trend occurred.

4.2.3. Australia

Figure 2 displays a marked decrease in albedo and increase in SINDVI in southeast Australia. Especially, the prominent declined in albedo by 0.118 from 2009 to 2011 was synchronous with a rapid enhancement in SINDVI (Figure 8f). The sudden rise of SINDVI was due to a strong La Niña event in early 2010, which resulted in incredibly high precipitation and large-scale flooding to the southeast Australia (van Dijk et al., 2013). From 1997 to 2009, southeast Australia suffered the driest period called the Millennium Drought (Aghakouchak et al., 2014). In this dry period, albedo maintained high with the average of 0.295 in the open shrub study area (Figure 8f). Grassland and desert are the dominant land cover in southeast Australia. In those areas, albedo is highly correlated with the vegetation. The increase in albedo will lead to less shortwave net radiation that eventually decreases the precipitation and dries the Earth. Finally, it forces the albedo to increase.

4.3. Limitations and Future Research

In the current study, snow cover and vegetation index are the factors were considered and estimated for the trend of albedo. However, the other parameters such as temperature, precipitation, and soil moisture (Guan et al., 2009) can also be important to influence the change of albedo. Unfortunately, due to the limitation of reliable high-resolution data on the global scale, the changes of these parameters have not been studied in the current research. However, we recognize the potential importance of other parameters. In the future studies, including of more parameters will clearly increase our understanding of the change of albedo.

5. Conclusions

In many areas, albedo and snow cover decreased but vegetation increased during the period of 2002 to 2016. From a global scale, MODIS albedo decreased by 0.0004 during the early 21st century. However, in Northern Hemisphere, albedo increased by 0.0009 in midlatitudes while decreased by 0.004 in high latitudes. The midlatitudes showed a characteristic variability for both albedo and snow cover, wherein the dramatic fluctuation of snow cover predominated the change of albedo. These areas included North America and Eastern Europe. Meanwhile, in Central Asia, widespread browning of vegetation made more contribution to the enhanced albedo.

Because snow cover considerably affects surface albedo, it is necessary to conduct further research to differentiate snow-covered and snow-free conditions. This will permit a better understanding of the impact of snow cover with respect to albedo variations. Snow-free albedo is also crucial for land surface models to evaluate the exchange of energy, among other things.

Acknowledgments
This work is jointly supported by the National Natural Science Foundation of China (41641058), the National Key Technology R&D Program of China (grant 2016YFC0500106), Special Project of Science and Technology Basic Work (grant 2014FY210800-5), and Chongqing R&D Project of the high technology and major industries ([2017]1231). We acknowledged NASA's MODIS Science Team for providing albedo, NDVI, and snow cover datasets. Albedo and vegetation Indices were obtained from the Land Processes Distributed Active Archive Center (LP DAAC) (https://lpdaac.usgs.gov/dataset_discovery); snow cover was obtained via NASA National Snow and Ice Data Center (http://nsidc.org/data/MOD10CM#). We thank NOAA Earth System Research Laboratory Physical Sciences Division for providing NCEP reanalysis climatology data via (https://www.esrl.noaa.gov/psd/data/gridded/data.ncep.reanalysis.html). We thank Dan Moore for helpful comments and revision of the manuscript. We also thank the Editor and three anonymous reviewers for their beneficial comments and suggestions.

References

Aghakouchak, A., Feldman, D., Stewardson, M. J., Saphores, J. D., Grant, S., & Sanders, B. (2014). Australia's drought: Lessons for California. *Science*, *343*(6178), 1430–1431. https://doi.org/10.1126/science.343.6178.1430

Betts, A. K., & Ball, J. H. (1997). Albedo over the boreal forest. *Journal of Geophysical Research*, *102*(D24), 28,901–28,909. https://doi.org/10.1029/96JD03876

Betts, R. A. (2000). Offset of the potential carbon sink from boreal forestation by decreases in surface albedo. *Nature*, *408*(6809), 187–190. https://doi.org/10.1038/35041545

Bintanja, R., & Krikken, F. (2016). Magnitude and pattern of Arctic warming governed by the seasonality of radiative forcing. *Scientific Reports*, *6*(1), 38287. https://doi.org/10.1038/srep38287

Blok, D., Schaepman-Strub, G., Bartholomeus, H., Heijmans, M. M. P. D., Maximov, T. C., & Berendse, F. (2011). The response of Arctic vegetation to the summer climate: Relation between shrub cover, NDVI, surface albedo and temperature. *Environmental Research Letters*, *6*(3), 035502. https://doi.org/10.1088/1748-9326/6/3/035502

Bonan, G. B. (1997). Effects of land use on the climate of the United States. *Climatic Change*, *37*(3), 449–486. https://doi.org/10.1023/A:1005305708775

Bonan, G. B., Iii, F. S. C., & Thompson, S. L. (1995). Boreal forest and tundra ecosystems as components of the climate system. *Climatic Change*, *29*(2), 145–167. https://doi.org/10.1007/BF01094014

Bounoua, L., Collatz, G. J., Los, S. O., Sellers, P. J., Dazlich, D. A., Tucker, C. J., & Randall, D. A. (2000). Sensitivity of climate to changes in NDVI. *Journal of Climate*, *13*(13), 2277–2292. https://doi.org/10.1175/1520-0442(2000)013%3C2277:SOCTCI%3E2.0.CO;2

Brovkin, V., Claussen, M., Driesschaert, E., Fichefet, T., Kicklighter, D., Loutre, M. F., … Sokolov, A. (2006). Biogeophysical effects of historical land cover changes simulated by six Earth system models of intermediate complexity. *Climate Dynamics*, *26*(6), 587–600. https://doi.org/10.1007/s00382-005-0092-6

Chapin, F. S., III, Sturm, M., Serreze, M. C., McFadden, J. P., Key, J. R., Lloyd, A. H., … Welker, J. M. (2005). Role of land-surface changes in arctic summer warming. *Science*, *310*(5748), 657–660. https://doi.org/10.1126/science.1117368

Chen, Z., Yin, Q., Li, L., & Xu, H. (2010). Ecosystem health assessment by using remote sensing derived data: A case study of terrestrial region along the coast in Zhejiang province. Geoscience and Remote Sensing Symposium.

Davin, E. L., & de Noblet-Ducoudré, N. (2010). Climatic impact of global-scale deforestation: Radiative versus nonradiative processes. *Journal of Climate*, *23*(1), 97–112. https://doi.org/10.1175/2009jcli3102.1

Dickinson, R. E. (1983). Land surface processes and climate—Surface albedos and energy balance. *Advances in Geophysics*, *25*(12), 305–353. https://doi.org/10.1016/S0065-2687(08)60176-4

Geng, G., Zhang, Q., Martin, R. V., van Donkelaar, A., Huo, H., Che, H., … He, K. (2015). Estimating long-term $PM_{2.5}$ concentrations in China using satellite-based aerosol optical depth and a chemical transport model. *Remote Sensing of Environment*, *166*, 262–270. https://doi.org/10.1016/j.rse.2015.05.016

Ghimire, B., Williams, C. A., Masek, J., Gao, F., Wang, Z., Schaaf, C., & He, T. (2014). Global albedo change and radiative cooling from anthropogenic land cover change, 1700 to 2005 based on MODIS, land use harmonization, radiative kernels, and reanalysis. *Geophysical Research Letters*, *41*, 9087–9096. https://doi.org/10.1002/2014GL061671

Govaerts, Y., & Lattanzio, A. (2008). Estimation of surface albedo increase during the eighties Sahel drought from Meteosat observations. *Global and Planetary Change*, *64*(3-4), 139–145. https://doi.org/10.1016/j.gloplacha.2008.04.004

Govindasamy, B., Duffy, P. B., & Caldeira, K. (2001). Land use changes and northern hemisphere cooling. *Geophysical Research Letters*, *28*(2), 291–294. https://doi.org/10.1029/2000GL006121

Guan, X., Huang, J., Guo, N., Bi, J., & Wang, G. (2009). Variability of soil moisture and its relationship with surface albedo and soil thermal parameters over the loess plateau. *Advances in Atmospheric Sciences*, *26*(4), 692–700. https://doi.org/10.1007/s00376-009-8198-0

He, T., Liang, S., & Song, D. X. (2015). Analysis of global land surface albedo climatology and spatial-temporal variation during 1981–2010 from multiple satellite products. *Journal of Geophysical Research: Atmospheres*, *119*, 10,281–10,298. https://doi.org/10.1002/2014JD021667

Hope, A. S., Boynton, W. L., Stow, D. A., & Douglas, D. C. (2003). Interannual growth dynamics of vegetation in the Kuparuk River watershed, Alaska based on the normalized difference vegetation index. *International Journal of Remote Sensing*, *24*(17), 3413–3425. https://doi.org/10.1080/0143116021000021170

Huete, A., Didan, K., Miura, T., Rodriguez, E. P., Gao, X., & Ferreira, L. G. (2002). Overview of the radiometric and biophysical performance of the MODIS vegetation indices. *Remote Sensing of Environment*, *83*(1-2), 195–213. https://doi.org/10.1016/S0034-4257(02)00096-2

Irwin, A. J., & Oliver, M. J. (2009). Are ocean deserts getting larger? *Geophysical Research Letters*, *36*, L18609. https://doi.org/10.1029/2009GL039883

Ji, F., Wu, Z., Huang, J., & Chassignet, E. P. (2014). Evolution of land surface air temperature trend. *Nature Climate Change*, *4*(6), 462–466. https://doi.org/10.1038/nclimate2223

Jin, Y. (2003). Consistency of MODIS surface bidirectional reflectance distribution function and albedo retrievals: 1. Algorithm performance. *Journal of Geophysical Research*, *108*(D5), 4159. https://doi.org/10.1029/2002JD002803

Jin, Y., Schaaf, C. B., Gao, F., Li, X., Strahler, A. H., Zeng, X., & Dickinson, R. E. (2002). How does snow impact the albedo of vegetated land surfaces as analyzed with MODIS data? *Geophysical Research Letters*, *29*(10), 1374. https://doi.org/10.1029/2001GL014132

Kalnay, E., Kanamitsu, M., Kistler, R., Collins, W., Deaven, D., Gandin, L., … Joseph, D. (1996). The NCEP/NCAR 40-year reanalysis project. *Bulletin of the American Meteorological Society*, *77*(3), 437–471. https://doi.org/10.1175/1520-0477(1996)077%3C0437:tnyrp%3E2.0.co;2

Khanna, J., Medvigy, D., Fueglistaler, S., & Walko, R. (2017). Regional dry-season climate changes due to three decades of Amazonian deforestation. *Nature Climate Change*, *7*(3), 200–204. https://doi.org/10.1038/nclimate3226

Kintisch, E. (2017). Meltdown. *Science*, *355*(6327), 788–791. https://doi.org/10.1126/science.355.6327.788

Lai, L., Huang, X., Yang, H., Chuai, X., Zhang, M., Zhong, T., … Thompson, J. R. (2016). Carbon emissions from land-use change and management in China between 1990 and 2010. *Science Advances*, *2*(11), e1601063–e1601063. https://doi.org/10.1126/sciadv.1601063

Liang, S. (2007). Recent developments in estimating land surface biogeophysical variables from optical remote sensing. *Progress in Physical Geography*, *31*(5), 501–516. https://doi.org/10.1177/0309133307084626

Liang, S., Wang, K., Zhang, X., & Wild, M. (2010). Review on estimation of land surface radiation and energy budgets from ground measurement, remote sensing and model simulations. *IEEE Journal of Selected Topics in Applied Earth Observations & Remote Sensing*, *3*(3), 225–240. https://doi.org/10.1109/JSTARS.2010.2048556

Liang, S., Zhang, X., He, T., Cheng, J., & Wang, D. (2013). Remote sensing of the land surface radiation budget. In G. P. Petropoulos (Ed.), *Remote sensing of energy fluxes and soil moisture content* (1st ed.pp. 121–162). Boca Raton, FA: CRC Press. https://doi.org/10.1201/b15610-7

Lioubimtseva, E., & Henebry, G. M. (2009). Climate and environmental change in arid Central Asia: Impacts, vulnerability, and adaptations. *Journal of Arid Environments*, *73*(11), 963–977. https://doi.org/10.1016/j.jaridenv.2009.04.022

Loarie, S. R., Lobell, D. B., Asner, G. P., Mu, Q. Z., & Field, C. B. (2011). Direct impacts on local climate of sugar-cane expansion in Brazil. *Nature Climate Change*, *1*(2), 105–109. https://doi.org/10.1038/nclimate1067

Lovell, J. L., & Graetz, R. D. (2001). Filtering pathfinder AVHRR land NDVI data for Australia. *International Journal of Remote Sensing*, *22*(13), 2649–2654. https://doi.org/10.1080/01431160116874

Lutz, S., Anesio, A. M., Raiswell, R., Edwards, A., Newton, R. J., Gill, F., & Benning, L. G. (2016). The biogeography of red snow microbiomes and their role in melting arctic glaciers. *Nature Communications*, *7*, 11968. https://doi.org/10.1038/ncomms11968

Ma, M., & Veroustraete, F. (2006). Reconstructing pathfinder AVHRR land NDVI time-series data for the Northwest of China. *Advances in Space Research*, *37*(4), 835–840. https://doi.org/10.1016/j.asr.2005.08.037

Moody, E. G., King, M. D., Schaaf, C. B., Hall, D. K., & Platnick, S. (2007). Northern Hemisphere five-year average (2000–2004) spectral albedos of surfaces in the presence of snow: Statistics computed from Terra MODIS land products. *Remote Sensing of Environment*, *111*(2-3), 337–345. https://doi.org/10.1016/j.rse.2007.03.026

NASA Land Processes Distributed Active Archive Center, U. E. C. (2016). MODIS land products quality assurance tutorial: Part-1.

Naudts, K., Chen, Y., Mcgrath, M. J., Ryder, J., Valade, A., Otto, J., & Luyssaert, S. (2016). Europe's forest management did not mitigate climate warming. *Science*, *351*(6273), 597–600. https://doi.org/10.1126/science.aad7270

Palmer, T. (2014). Record-breaking winters and global climate change. *Science*, *344*(6186), 803–804. https://doi.org/10.1126/science.1255147

Peng, J., Chen, S., Lü, H., Liu, Y., & Wu, J. (2016). Spatiotemporal patterns of remotely sensed $PM_{2.5}$ concentration in China from 1999 to 2011. *Remote Sensing of Environment*, *174*, 109–121. https://doi.org/10.1016/j.rse.2015.12.008

Piao, S., Mohammat, A., Fang, J., Cai, Q., & Feng, J. (2006). NDVI-based increase in growth of temperate grasslands and its responses to climate changes in China. *Global Environmental Change*, *16*(4), 340–348. https://doi.org/10.1016/j.gloenvcha.2006.02.002

Planque, C., Carrer, D., & Roujean, J.-L. (2017). Analysis of MODIS albedo changes over steady woody covers in France during the period of 2001–2013. *Remote Sensing of Environment*, *191*, 13–29. https://doi.org/10.1016/j.rse.2016.12.019

Qu, X., & Hall, A. (2007). What controls the strength of snow-albedo feedback? *Journal of Climate*, *20*(15), 3971–3981. https://doi.org/10.1175/jcli4186.1

Sanchez-Lorenzo, A., Enriquez-Alonso, A., Wild, M., Trentmann, J., Vicente-Serrano, S. M., Sanchez-Romero, A., … Hakuba, M. Z. (2017). Trends in downward surface solar radiation from satellites and ground observations over Europe during 1983–2010. *Remote Sensing of Environment*, *189*, 108–117. https://doi.org/10.1016/j.rse.2016.11.018

Schaaf, C., Martonchik, J., Pinty, B., Govaerts, Y., Gao, F., Lattanzio, A., … Taberner, M. (2008). Retrieval of surface albedo from satellite sensors, In S. Liang (Eds.), *Advances in land remote sensing* (pp. 219–243). Dordrecht, Netherlands: Springer. https://doi.org/10.1007/978-1-4020-6450-0_9

Sigmond, M., & Fyfe, J. C. (2016). Tropical Pacific impacts on cooling North American winters. *Nature Climate Change*, *6*(10), 970–974. https://doi.org/10.1038/nclimate3069

Sturm, D., Daeschner, S., Hope, A., Douglas, D., Petersen, A., Myneni, R., … Oechel, W. (2003). Variability of the seasonally integrated normalized difference vegetation index across the north slope of Alaska in the 1990s. *International Journal of Remote Sensing*, *24*(5), 1111–1117. https://doi.org/10.1080/0143116021000020144

Sturm, M. (2005). Changing snow and shrub conditions affect albedo with global implications. *Journal of Geophysical Research*, *110*, G01004. https://doi.org/10.1029/2005JG000013

Thackeray, C. W., & Fletcher, C. G. (2016). Snow albedo feedback: Current knowledge, importance, outstanding issues and future directions. *Progress in Physical Geography*, *40*(3), 392–408. https://doi.org/10.1177/0309133315620999

Trenberth, K. E. (2011). Changes in precipitation with climate change. *Climate Research*, *47*(1), 123–138. https://doi.org/10.3354/cr00953

United Nations Economic Committee for Europe, F (2011). The European forest sector outlook study II, 2010–2030. *Geneva Timber & Forest Study Papers*, *4*, 372.

van Dijk, A. I. J. M., Beck, H. E., Crosbie, R. S., de Jeu, R. A. M., Liu, Y. Y., Podger, G. M., … Viney, N. R. (2013). The Millennium Drought in southeast Australia (2001-2009): Natural and human causes and implications for water resources, ecosystems, economy, and society. *Water Resources Research*, *49*(2), 1040–1057. https://doi.org/10.1002/wrcr.20123

Verhoef, W., Menenti, M., & Azzali, S. (1996). Cover A colour composite of NOAA-AVHRR-NDVI based on time series analysis (1981–1992). *International Journal of Remote Sensing*, *17*(2), 231–235. https://doi.org/10.1080/01431169608949001

Viterbo, P., & Betts, A. K. (1999). Impact on ECMWF forecasts of changes to the albedo of the boreal forests in the presence of snow. *Journal of Geophysical Research*, *104*(D22), 27,803–27,810. https://doi.org/10.1029/1998JD200076

Wielicki, B. A., Wong, T., Loeb, N., Minnis, P., Priestley, K., & Kandel, R. (2005). Changes in Earth's albedo measured by satellite. *Science*, *308*(5723), 825. https://doi.org/10.1126/science.1106484

Xiao, J., Zhou, Y., & Zhang, L. (2015). Contributions of natural and human factors to increases in vegetation productivity in China. *Ecosphere*, *6*(11), art233. https://doi.org/10.1890/es14-00394.1

Yang, F., Kumar, A., Wang, W., Juang, H. M. H., & Kanamitsu, M. (2001). Snow-Albedo Feedback and Seasonal Climate Variability over North America. *Journal of Climate*, *14*(22), 4245–4248. https://doi.org/10.1175/1520-0442(2001)014<4245:SAFASC>2.0.CO;2

Yu, B., & Zhang, X. (2015). A physical analysis of the severe 2013/2014 cold winter in North America. *Journal of Geophysical Research: Atmospheres*, *120*, 10,149–10,165. https://doi.org/10.1002/2015JD023116

Zhai, J., Liu, R., Liu, J., Zhao, G., & Huang, L. (2014). Radiative forcing over China due to albedo change caused by land cover change during 1990–2010. *Journal of Geographical Sciences*, *24*(5), 789–801. https://doi.org/10.1007/s11442-014-1120-4

Zhang, M., Huang, X., Chuai, X., Yang, H., Li, L., & Tan, J. (2015). Impact of land use type conversion on carbon storage in terrestrial ecosystems of China: A spatial-temporal perspective. *Scientific Reports*, *5*(1), 10233. https://doi.org/10.1038/srep10233

Zhang, X., Liang, S., Wang, K., Li, L., & Gui, S. (2010). Analysis of global land surface shortwave broadband albedo from multiple data sources. *IEEE Journal of Selected Topics in Applied Earth Observations and Remote Sensing*, *3*(3), 296–305. https://doi.org/10.1109/jstars.2010.2049342

Zhou, L., Tucker, C. J., Kaufmann, R. K., Slayback, D., Shabanov, N. V., & Myneni, R. B. (2001). Variations in northern vegetation activity inferred from satellite data of vegetation index during 1981 to 1999. *Journal of Geophysical Research*, *106*(D17), 20,069–20,083. https://doi.org/10.1029/2000JD000115